Mon. Not. R. Astron. Soc. **283,** 821–829 (1996)

Analysis of Keck high-resolution spectra of VB 10

Andreas Schweitzer,[1★]† Peter H. Hauschildt,[1★]‡ France Allard[2★] and G. Basri[3★]

[1] *Department of Physics and Astronomy, Arizona State University, Tempe, AZ 85287-1504, USA*
[2] *Department of Physics, Wichita State University, Wichita, KS 67260-0032, USA*
[3] *Department of Astronomy, University of California, Berkeley, CA 94705, USA*

Accepted 1996 July 8. Received 1996 July 2; in original form 1996 April 19

ABSTRACT

We use a preliminary version of our 'NextGen' grid of cool star model atmospheres to compute synthetic line profiles which fit high-resolution Keck spectra of the cool M dwarf VB 10 satisfactorily well. We show that the parameters derived from the Keck data are consistent with the parameters derived from lower resolution spectra with larger wavelength coverage. We discuss the treatment of van der Waals broadening in cool stellar atmospheres that are dominated by molecules (mostly H_2). The line profiles are dominated by van der Waals pressure broadening and are a sensitive indicator for the gravity and metallicity. Therefore the high-resolution Keck spectra are useful for determining the parameters of M dwarfs. There is some ambiguity between the metallicity and gravity. For VB 10, we find from the high-resolution spectra that $5.0 < \log g < 5.5$ and $0 < [\mathrm{M/H}] < +0.5$ for an adopted fixed effective temperature of 2700 K, which is consistent with recent interior calculations.

Key words: atomic processes – line: profiles – stars: atmospheres – stars: fundamental parameters – stars: individual: VB 10 – stars: low-mass, brown dwarfs.

1 INTRODUCTION

M dwarfs are among the faintest and coolest stellar objects. Their spectra are dominated by molecular band absorption. In the optical region the major opacity sources are the TiO bands, which produce a pseudo-continuum with the atomic lines superposed. These atomic lines show very broad wings due to van der Waals broadening, whereas the molecular lines show only relatively small damping wings. We have recently obtained a high-resolution optical spectrum of the dM8e star VB 10 (Gl 752B) with the HIRES echelle on the Keck telescope. The collection and reduction of the data are as in Basri & Marcy (1995). In this paper, we use this spectrum to check our treatment of the van der Waals line broadening in M dwarf atmospheres and to estimate the gravity and the chemical composition of VB 10. VB 10 is known to be a chromospherically active flare star. However, in this paper we will neglect the chromosphere and will not attempt to model chromospheric spectral features, such as core emission observed in resonance lines.

Our calculations are based on a preliminary version of our latest grid of model atmospheres (the 'NextGen' or 'version 5' grid) for cool dwarf stars and version 6.2 of the generalized stellar atmosphere code PHOENIX. An important improvement over the previous generation of this grid (Allard & Hauschildt 1995, hereafter AH95) is larger and more reliable molecular line lists which allow us to compute detailed molecular line profiles. A complete description of all changes and improvements over the AH95 version of the models will be given in a subsequent paper (Allard, Hauschildt & Schweitzer, in preparation, hereafter AHS96). Note that we use metallicities scaled from the solar values of Anders & Grevesse (1989) and we use the notation

$$\left[\frac{\mathrm{M}}{\mathrm{H}}\right] := \log\left[\frac{\mathrm{M/H}}{\mathrm{M_\odot/H_\odot}}\right]$$

to specify abundances.

A previous analysis based on low-resolution spectra by Brett (1995) yielded only rough values for effective temperatures $T_{\rm eff} = 2400$–2600 K, $\log g \approx 5.0$ and $[\mathrm{M/H}] \approx 0.0$. Interior calculations (e.g. Burrows et al. 1993) require, for solar M dwarfs in the effective temperature range of ≈2700 K, gravities of $\log g \approx 5.3$.

In the next section we will describe our theoretical approach to the problem. We will discuss the basic approximation that we use as well as its numerical realization. In Section 3 we will present the results of our modelling. We will discuss the sensitivities of the profiles and try to establish error limits. In Section 4 we will compare the observed high-resolution spectra of VB 10 with our model spectra.

2 THE TREATMENT OF LINE BROADENING

2.1 The line profiles

We include all common line broadening mechanisms, i.e. thermal broadening, micro-turbulence, natural broadening and pressure

*E-mail: andy@sara.la.asu.edu (AS); yeti@hal.physast.uga.edu (PHH); allard@eureka.physics.twsu.edu (FA); basri@astra.berkeley.edu (GB)
†Present address: Landessternwarte, Königstuhl, D–69117 Heidelberg, Germany.
‡Present address: Department of Physics and Astronomy, The University of Georgia, Athens, GA 30602-2451, USA.

broadening, in both the model calculations and synthetic spectra. The resulting Voigt profiles $V(u,\alpha)$, where $u = \Delta\lambda/\Delta\lambda_D$ and $\alpha = (\lambda^2\gamma/4\pi c)/\Delta\lambda_D$ (λ_D is the Doppler width, γ the Lorentz width, $\Delta\lambda$ the distance from the line centre and λ the wavelength), are calculated as a convolution of a Gaussian and a Lorentz profile using standard approximations (e.g. Baschek & Scholz 1982). The gas temperatures in M dwarf atmospheres are not high enough to sustain a significant amount of ionization in the atmosphere. The electron and proton densities are, therefore, much smaller than the densities of the most important neutral and molecular species. Consequently, the contribution of Stark broadening to the total damping constant is very small, even in stars with very low metallicities. We include a microturbulence of $\xi = 2\ \mathrm{km\,s^{-1}}$ in addition to the thermal speed of the atoms and molecules. However, the total thermal plus microturbulent linewidths are for most lines much smaller than the linewidth due to van der Waals (vdW) broadening. In the following paragraphs we will describe in some detail the way in which we estimate the vdW damping constants and how their choice influences the computed profiles of both atomic and molecular lines. The interaction between two different, unpolarized, neutral particles is described by the van der Waals interaction

$$\Delta\nu = \frac{C_6}{r^6}, \tag{1}$$

where $\Delta\nu$ is the resulting frequency shift due to one interaction, r the relative distance between the interacting particles and C_6 the interaction constant for the vdW interaction. Within the impact or static approximation, vdW damping leads to a Lorentz profile with a full width to half-maximum damping constant γ_{vdW} (c.g.s. units):

$$\gamma_{vdW} = 17 C_6^{2/5} v^{3/5} N_p. \tag{2}$$

Here v is the relative velocity between perturber and absorber and N_p the number density of the perturber.

We base the calculation of C_6 on Unsöld's hydrogenic approximation (Unsöld 1955). However, we explicitly account for the different polarizabilities of each perturber in the equation for C_6 which leads to

$$C_6^0 = \frac{\alpha_p}{\alpha_H} 1.01 \times 10^{-32} (Z+1)^2 \times \left[\frac{E_H^2}{(E-E_l)^2} - \frac{E_H^2}{(E-E_u)^2}\right] \mathrm{cm^6\,s^{-1}}, \tag{3}$$

Table 1. The perturbers included in the calculations and their polarizabilities. The percentages are taken from models with $\log g = 5.0$, [M/H] = 0.0 and the respective T_{eff}. We chose the optical depth $\tau_{std} = 1$ [$d\tau_{std} = \kappa ds$ where κ is the absorption coefficient at a standard wavelength of 1.2 μm (AH95) and ds the geometric depth] as an example for an average line forming depth. The percentages are rounded on the last figure.

Perturber	α_p in 10^{-24} cm^3	Fraction of P_{gas} in per cent at $\tau_{std} = 1$ for $T_{eff} = 2000$	$T_{eff} = 2700$	$T_{eff} = 3500$
H	0.666793	1.2	14.9	66.6
He	0.204956	16.2	15.1	10.7
Ne	0.3956 ± 0.1%	0.02	0.02	0.01
Fe	8.4 ± 25%	0.01	0.01	≈0.005
H_2	0.806 ± 0.5%	82.4	69.8	22.4
CO	1.95 ± 0.5%	0.06	0.06	0.04
H_2O	1.45 ± 0.5%	0.07	0.06	0.01
N_2	1.7403 ± 0.5%	0.01	0.01	≈0.004

where α_p is the polarizability of the perturber, Z the charge of the absorber, E the ionization potential, E_l the lower and E_u the upper level excitation energy of the absorber, α_H the polarizability of hydrogen, and $E_H = 13.6\,\mathrm{eV}$. We include the most abundant perturbers in M dwarfs and their polarizabilities as given in Weast (1988) and listed in Table 1 to calculate the total van der Waals damping constant:

$$\gamma_{vdW}^{tot} = \sum_p \gamma_{vdW}^p, \tag{4}$$

where we sum over all perturbers considered. Due to the lack of availability of any vdW broadening mechanisms for molecules in this temperature range, we also use this approximation for the molecular lines.

Earlier investigations (Weidemann 1955) showed that the values as calculated by equation (3) are in good agreement with observed linewidths for alkali metals but not for other elements, such as iron (Kusch 1958). This has led to the introduction of correction factors to the 'classical' formula. Therefore we include a correction factor for C_6 of

$$C_6 = C_6^{corr} \times C_6^0 = 10^{1.8} \times C_6^0 \tag{5}$$

as described in Wehrese & Liebert (1980) for non-alkali-like species. For alkali metals and ions with alkali-like electron structure we omit any correction factor. This will be discussed and investigated in greater detail in Sections 4 and 5. However, as these results will show, the value of the correction factor is not well determined for the non-alkali-like species.

2.2 The numerical treatment of vdW broadening

In order to calculate the emerging spectrum we have to calculate a Voigt profile at every wavelength point for every line at every depth point. To limit the computation time we make the following simplification.

Before calculating the absorption coefficient, a line selection procedure decides which lines are calculated with Voigt profiles. We follow the line selection procedure described by AH95. Only lines that are stronger than a certain threshold relative to the continuum are treated with Voigt profiles. This is decided by comparing the absorption coefficient at the line centre κ_l with the corresponding continuous absorption coefficient κ_c. Only if the ratio $\Gamma = \kappa_l/\kappa_c$ for at least one of three representative depth points is larger than a pre-set threshold value is a line treated with a Voigt profile. Otherwise the line is considered so weak that to a good approximation it can be treated as a Gaussian profile in order to save computation time. The number of considered atomic lines is much smaller than the number of molecular lines. This allows us to set Γ for atomic lines to be very low in order to treat as many lines as possible with Voigt profiles. The number of molecular lines is about two orders of magnitude larger but, since the atmospheric structure does not change significantly (as test calculations showed) with the inclusion of more Voigt profiles for molecular lines, we set the threshold for molecular lines for iterations to $\Gamma = 100$. For high-resolution spectra we use lower values (usually $\Gamma \approx 1$), although we found that the spectra do not change significantly by increasing the number of lines with Voigt profiles.

The spectra presented throughout this paper used $\Gamma = 5$ when we examined atomic lines and $\Gamma = 0.1$ when we examined molecular lines. All the spectra are furthermore based on self-consistent model structures with their respective parameters.

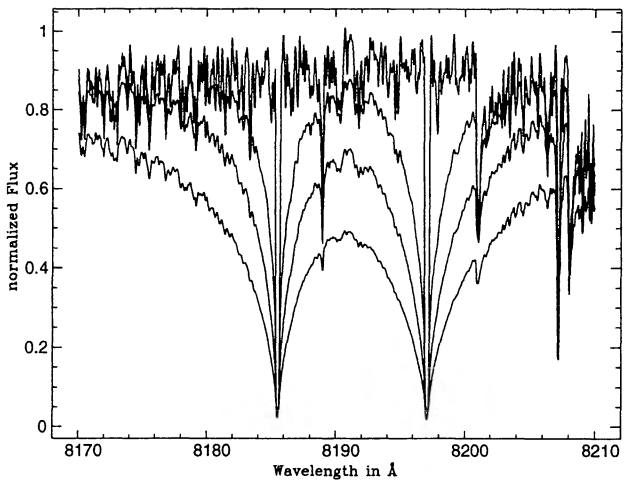

Figure 1. The calculated Na I λλ8183, 8195 doublet in vacuum with different broadening mechanisms ($\log g = 5.0$, $T_{\rm eff} = 2700$ K, [M/H] = 0.0). From top to bottom: Gaussian profile; only H and He as perturbers; H, He and H_2 as perturbers; perturbers of Table 1 without the correction factor (this plot is lying exactly on the previous one); perturbers of Table 1 and the correction factor of $10^{1.8}$ artificially applied.

3 RESULTS

3.1 Synthetic line profiles

To demonstrate the various effects influencing the line profiles we will use the Na I λλ8183, 8195 subordinate doublet and the K I λλ7665, 7699 resonance doublet, since they are available in the Keck spectra (see Section 4). Note that the synthetic line profiles in this section are shown at their *vacuum* wavelengths.

Equation (2) shows that the vdW damping constant is a linear function of the perturber density. This implies that the major contribution to the total vdW broadening will be due to the effect of the most abundant perturbers, namely H I, He I and H_2, because the polarizabilities change much less than the relative concentrations of the perturbing species (cf. Table 1). In Fig. 1 we show the influence of H_2 on the profile of the subordinate Na I λλ8183, 8195 doublet. All the other perturbers listed in Table 1 do not contribute significantly to the linewidth; the profile is identical to the one that is only H–He–H_2 broadened. This is valid even for metal abundances higher than solar.

In addition, Fig. 1 shows the effect of the correction factor introduced in equation (5) by artificially applying it to the alkali metal sodium. In this case the correction factor is only applied to demonstrate the uncertainty which still is present in the vdW damping constant. A final decision on the validity of such a factor has to be made by comparing the synthetic profiles with observations.

Changes of the absolute number density of each perturber will change the damping constant. We consider two ways to change the perturber densities: changing the gravity or changing the metallicity. Higher surface gravities will increase the total pressure in every layer of the atmosphere. This will also increase the number density of every perturber for constant metallicity. An example of the gravity effect on the linewidths is shown in Fig. 2 which illustrates the influence of $\log g$ on the profile of the subordinate Na I doublet as well on the K I λλ7665, 7699 resonance doublet for model atmospheres with $T_{\rm eff} = 2700$ K, solar metallicity and a difference in the gravities of the one order of magnitude.

On the other hand, an increase in metallicity at constant gravity will decrease both the total pressure and the number density of the main perturbers, H I, He I and H_2. It furthermore will bind hydrogen in hydrides and water vapour. Therefore all these effects will make the line wings narrower. We demonstrate this in Fig. 3, with the same two doublets as above. The only difference in the models shown is half an order of magnitude in the metallicity.

This introduces the problem that small changes in metallicity can be compensated for by changes in the gravity, thus making the determination of both parameters from the wings of strong lines alone questionable. This means that abundance analyses of cool dwarfs in general must be performed with caution, and simple techniques may lead to errors. This will be investigated in much more detail in subsequent work.

3.2 Comparison with other methods

To demonstrate the improvement brought by the present treatment, we will briefly review other commonly used methods: (1) the Unsöld formula without perturber correction used by Allard (1990) and AH95, and (2) using the pre-calculated damping

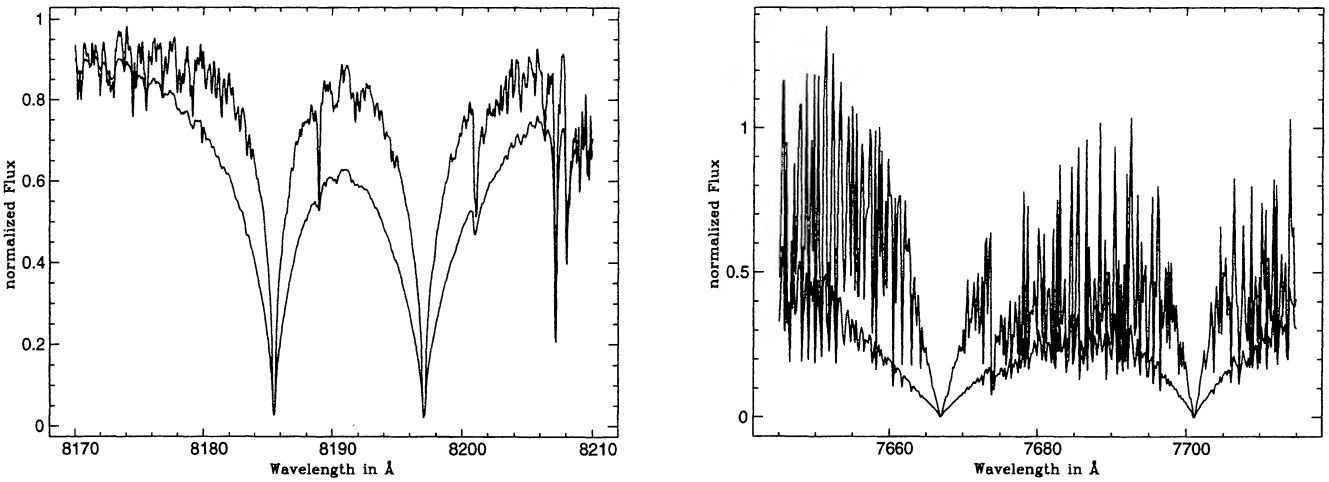

Figure 2. The calculated Na I λλ8183, 8195 and K I λλ7665, 7699 doublets in vacuum for $\log g = 4.5$ (upper line) and $\log g = 5.5$ (lower line) ($T_{\rm eff} = 2700$ K, [M/H] = 0.0).

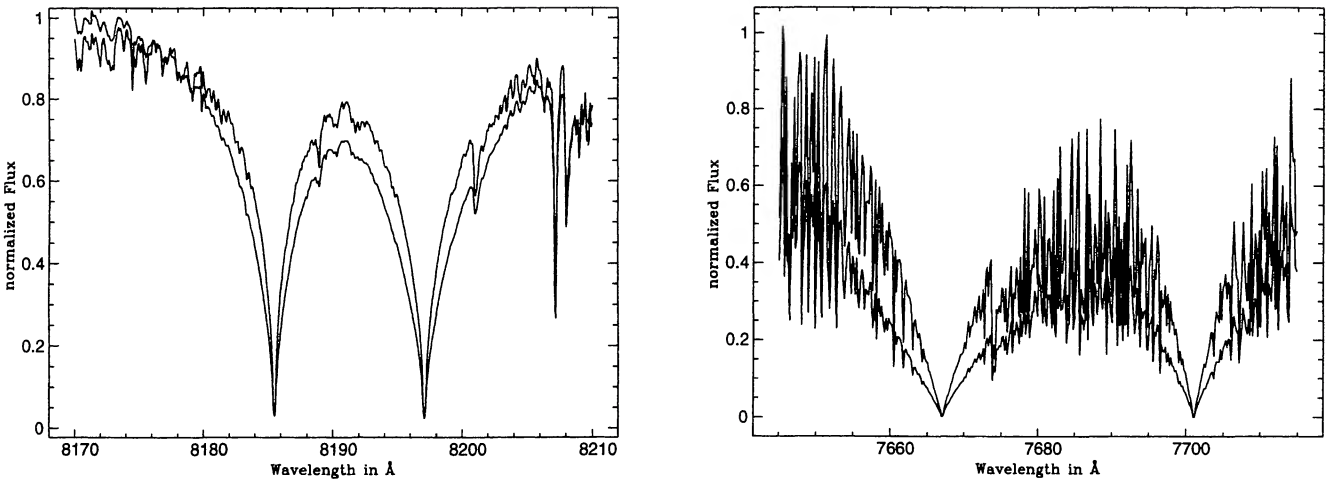

Figure 3. The calculated Na I λλ8183, 8195 and K I λλ7665, 7699 doublets in vacuum for [M/H] = 0.5 (upper line) and [M/H] = 0.0 (lower line) ($T_{\rm eff}$ = 2700 K, $\log g$ = 5.5).

constants per hydrogen atom at 10 000 K provided on CD-ROM No.1 by Kurucz (1994).

The method (1) uses an average broadening mechanism by taking the total particle density instead of the density of every perturber and by not distinguishing between the different perturbers, i.e. not taking into account the different polarizabilities and reduced masses, the latter influencing the relative velocity in equation (2). In addition, it uses the correction factor for all lines.

In Fig. 4 we compare the same Na I λλ8183, 8195 profiles as above calculated with the old method with those calculated with the new method but with the correction factor artificially applied for comparison. As can be seen there are clear differences between the two methods. The new method results in narrower lines since it accounts for the different polarizabilities and reduced masses which decrease C_6 in equation (3) or $\gamma_{\rm vdW}$ in equation (2) compared with C_6 and $\gamma_{\rm vdW}$ calculated as described above, and therefore also decreases the damping constants of equation (4).

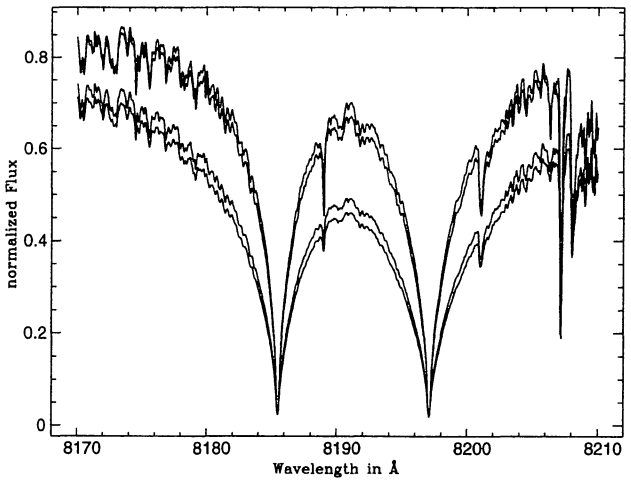

Figure 4. The calculated Na I λλ8183, 8195 doublet in vacuum with different broadening methods ($\log g$ = 5.0, $T_{\rm eff}$ = 2700 K, [M/H] = 0.0). From top to bottom: our method without the correction factor; using Kurucz's damping constant per hydrogen atom at 10 000 K; our method and the correction factor of $10^{1.8}$ artificially applied; the old method. See Section 3.2 for details.

In Fig. 4 we also plot the profiles using the damping constants provided by Kurucz. We find only small differences between Kurucz's vdW damping constant and ours, if we omit the correction factor. In test calculations we also compared the use of natural damping constants provided by Kurucz with those calculated with the classical approximation. Since the total linewidth in M dwarfs is dominated by vdW broadening, it makes little observable difference which treatment of natural damping is employed to model their spectra. We adopt our own methods in the following discussion.

We furthermore compared directly the damping constants obtained with our approximation with the corresponding values from Kurucz's list and found only small differences for the vast majority of the lines above 6000 Å. The largest differences arise from the correction factor that we included for non-alkali species. For the UV region the differences are larger. Here the hydrogenic approximation for the absorber that we used differs substantially from the method that Kurucz used. This does not affect the spectra we present here. In general, the photospheric UV flux from M dwarfs is negligible. However, a more thorough investigation must be performed for stars that are significantly hotter than M stars.

3.3 Uncertainties in the broadening mechanism of molecular lines

As can be seen from Figs 5 and 11 (later) the molecular lines are much narrower than the atomic lines, both in the observations (cf. Section 4.6) and in our models. This is due to the fact that each molecular line is very weak compared with the strong atomic lines. Therefore only the Gaussian cores remain visible in the spectra and the linewidth is only the linewidth of the Gaussian core. Nevertheless, the Voigt profiles need to be included since they lift the Gaussian cores significantly without changing the linewidth, as corresponding comparisons have shown. In addition, the molecular lines lie so densely together that only their cores can remain visible; any wing contribution will effectively be blocked by the cores of neighbouring molecular lines. This means that the total width of molecular *features* is not as much dominated by the wings of the vdW broadening as for the atomic lines.

In order to estimate the error resulting from our approximations, we performed test calculations in which we omitted the correction

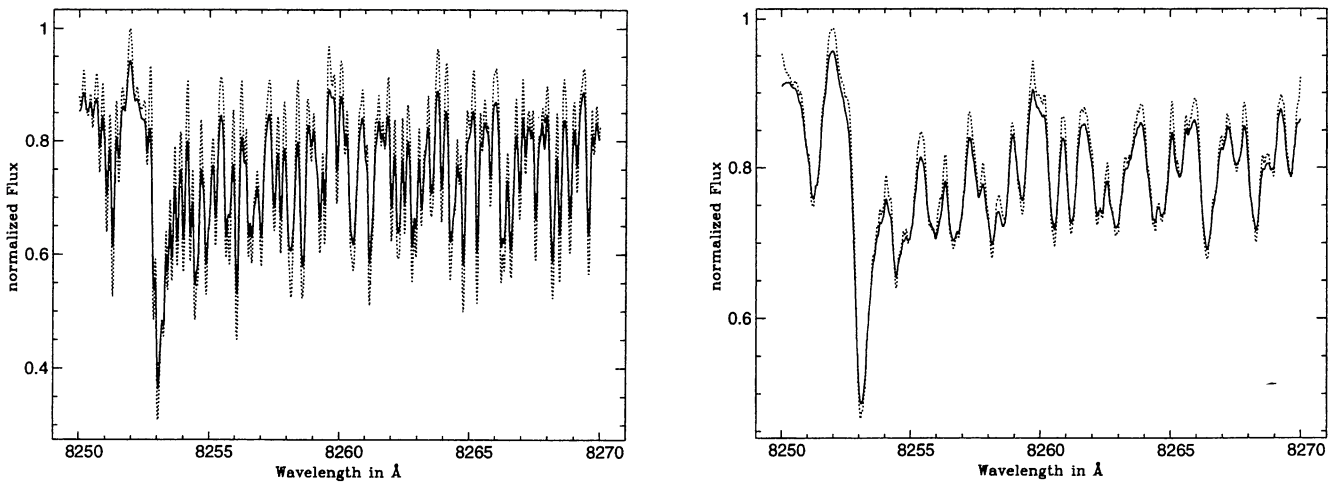

Figure 5. Calculated molecular lines for $\log g = 5.0$, [M/H] = +0.5, $T_{\rm eff} = 2600$ K. Dotted: without the artificial correction factor of $10^{1.8}$, solid: with the correction factor applied. Left panel: not rotationally broadened. Right panel: rotationally broadened with 10 km s^{-1}.

factor from equation (5) for molecules, which results in a change in the interaction constant by nearly 2 orders of magnitude. In contrast to the atomic lines (cf. Section 3.1 and Fig. 1), we found only small differences in the overall appearance of molecular lines in the optical (see Fig. 5), since only the line wings change and they are completely blended in the spectrum.

The most important result, however, was the influence of rotational broadening on the appearance of the molecular lines, which can be seen in Fig. 5 as well. As we applied rotational broadening to our test spectra, we found that even a small rotational velocity will broaden the lines so much that the uncertainties in the vdW broadening become unimportant. Only the cores of the stronger molecular lines remain visible. Also the influence of the gravity and metallicity becomes less important. We furthermore found that the effect of rotational broadening rises continuously with increasing rotational velocity. As a consequence, the molecular line 'haze' reveals a possibility to measure accurately the rotational velocity, as the haze is very sensitive to it (see Section 4.6).

4 COMPARISON OF VB 10 HIGH-RESOLUTION KECK SPECTRA WITH SYNTHETIC SPECTRA

Our observation of VB 10 was obtained with the HIRES echelle on the Keck telescope during a run on 1995 March 12 under clear conditions. Our exposure time was 30 min with 0.8-arcsec seeing. The instrumental setup and data reduction were very similar to those described by Basri & Marcy (1995). The wavelength setting was slightly modified to include the subordinate Na I λλ8183, 8195 doublet, the K I λλ7665, 7699 resonance doublet, the Ca I λ6573 resonance line, the Ba I λ7911 resonance line and the Fe I λ7913, Fe I λ8662 and Fe I λ8689 subordinate lines. Inclusion of Na I meant that we could not also observe the Rb I line discussed by Basri & Marcy (1995).

We consider models with any combination of $\log g = 4.0, 4.5, 5.0, 5.5$ and scaled solar metallicities [M/H] = −0.5, 0.0, +0.5. For the purpose of this paper, we adopt a fixed effective temperature of 2700 K for VB 10, derived from fitting low-resolution spectra

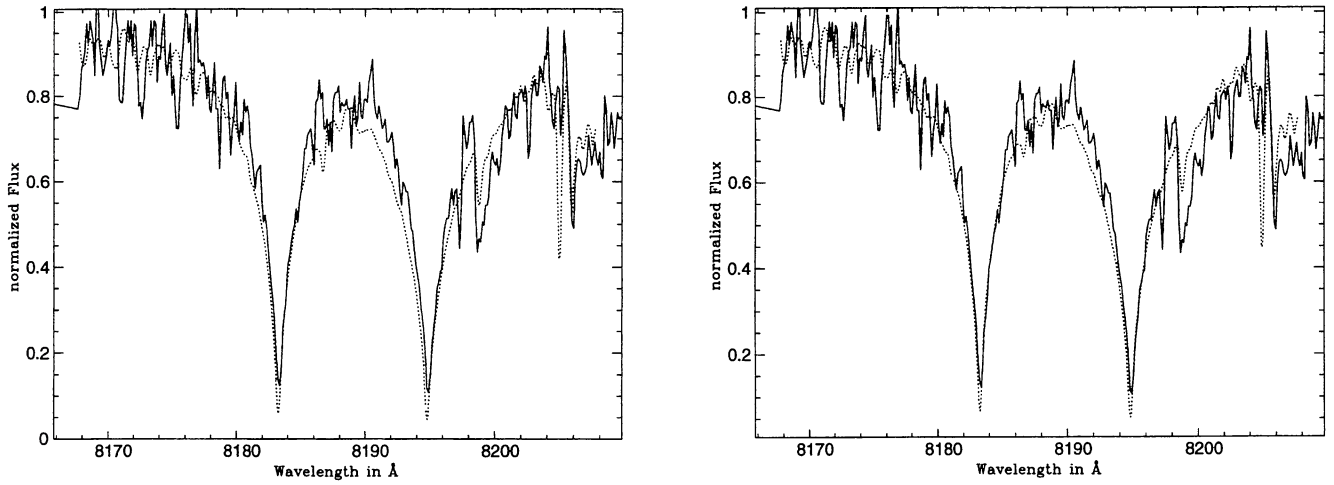

Figure 6. The fit to the Na I λλ8183, 8195 doublet. Solid: observed. Dotted: $T_{\rm eff} = 2700$ K, $\log g = 5.0$, [M/H] = 0.0 (left); and $T_{\rm eff} = 2700$ K, $\log g = 5.5$, [M/H] = +0.5 (right). Both models are rotationally broadened by 8 km s^{-1}.

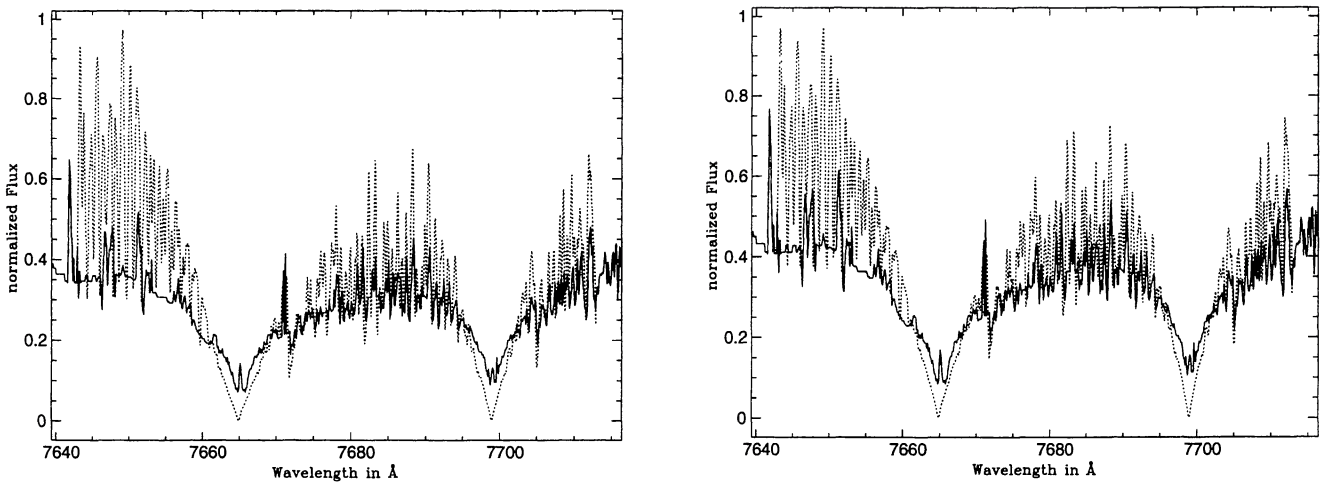

Figure 7. The fit to the K I λλ7665, 7699 doublet. Solid: observed. Dotted: $T_{\rm eff} = 2700$ K, $\log g = 5.0$, [M/H] = 0.0 (left); and $T_{\rm eff} = 2700$ K, $\log g = 5.5$, [M/H] = +0.5 (right). Both models are rotationally broadened by 8 km s^{-1}.

obtained by Kirkpatrick et al. (1993) and Jones et al. (1994) to low-resolution models (see Schweitzer 1995). It is not the purpose of this paper to investigate the influence of the effective temperature on the line profile. This will be done in subsequent work where the parameters will be verified or revised, if necessary. A rotational velocity of 8 km s^{-1} was adopted, using the method of Basri & Marcy (1995). We reconsider this in Section 4.6. Due to the complexity of the spectra we performed the fits and decided on their quality by eye.

4.1 The sodium doublet

The Na I λλ8183, 8195 doublet lines are subordinate transitions and, therefore, form mainly in the photosphere and should not be significantly affected by the chromosphere of VB 10. Our best fits are the two models with $\log g = 5.0$ and [M/H] = 0.0 and with $\log g = 5.5$ and [M/H] = +0.5, shown in Fig. 6. There are no significant differences in the appearance of the two model spectra, although the parameters differ substantially. This demonstrates the effect mentioned above, namely that an increase in metallicity decreases the number density of the major perturbers, H I, He I and H_2, and thus partly cancels the effect of increasing the gravity, in particular for strong lines. This shows that one has to be very careful when analysing M dwarf spectra in detail. In our case here, we found good agreement between observation and models for parameters within the intervals $5.0 < \log g < 5.5$ and $0.0 <$ [M/H] $< +0.5$. We therefore use this as an error limit on our analyses. For any parameter combination beyond these intervals we find no reasonable agreement.

The synthetic line profiles show a deeper core than the observed lines. We calculated several models with a different microturbulence in order to 'fill in' the core, but we found no significant improvement to the fit. The remaining difference is most likely due to non-local thermodynamic equilibrium (NLTE) effects which might make line cores less deep. This will be investigated in detail in future work (see e.g. Hauschildt et al. 1996). NLTE effects will have to be considered as they are highly non-linear and are very likely to affect the cores of strong lines.

We would also like to point out the numerous weak lines in the wings of the atomic lines. These are mostly TiO lines which are also visible in the observed spectrum and are not to be considered as noise (see also below, Section 4.6).

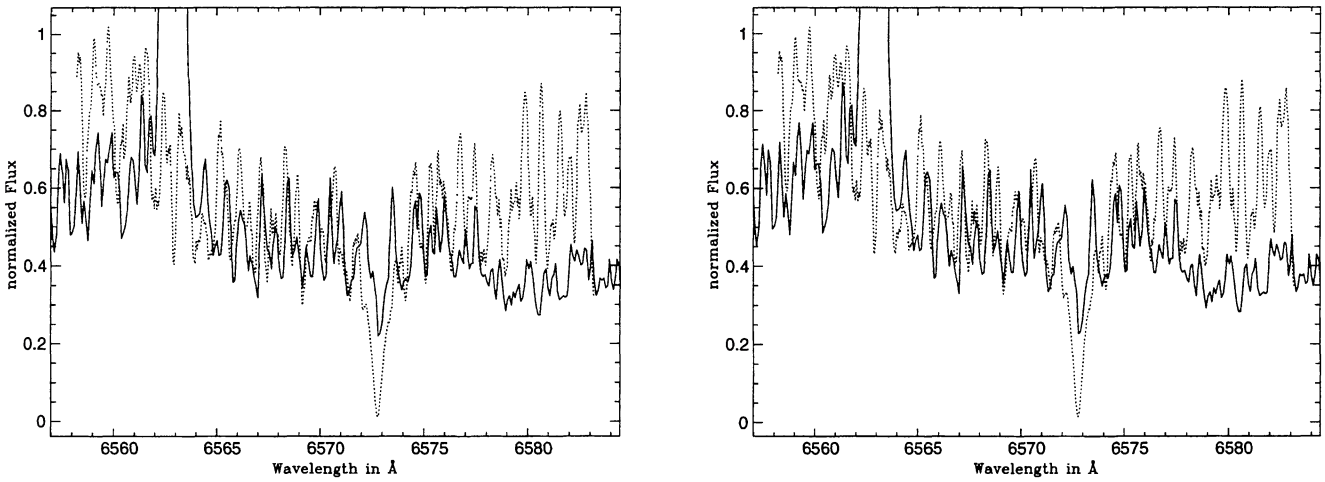

Figure 8. The fit to the Ca I λ6573 line. Solid: observed. Dotted: $T_{\rm eff} = 2700$ K, $\log g = 5.0$, [M/H] = 0.0 (left); and $T_{\rm eff} = 2700$ K, $\log g = 5.5$, [M/H] = +0.5 (right). Both models are rotationally broadened by 8 km s^{-1}. Note Hα in emission.

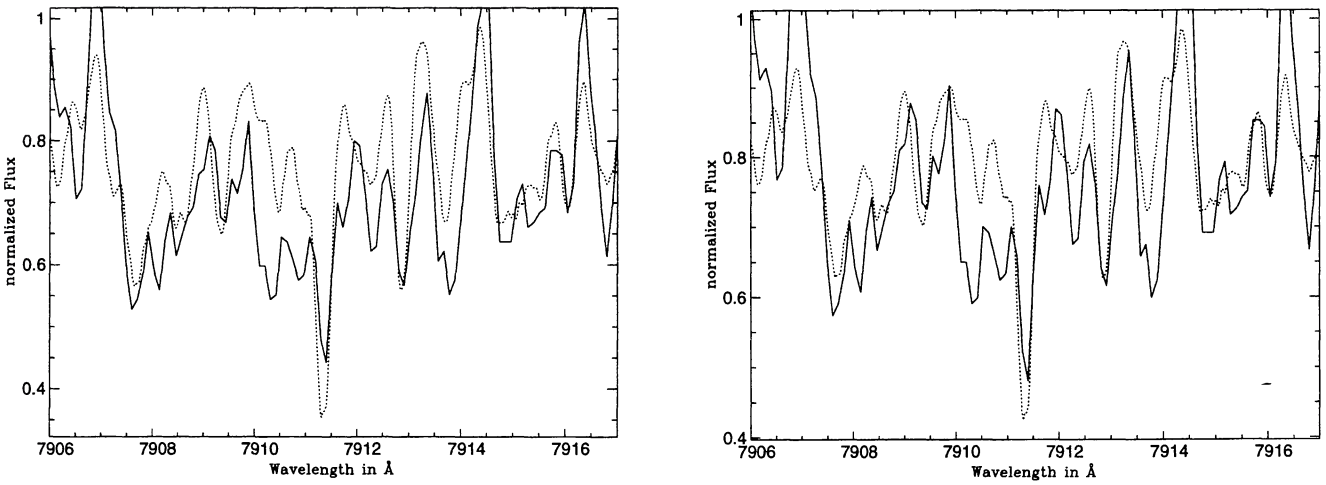

Figure 9. The fit to the Ba I λ7911 and Fe I λ7913 lines. Solid: observed. Dotted: $T_{\rm eff} = 2700$ K, $\log g = 5.0$, [M/H] = 0.0 (left); and $T_{\rm eff} = 2700$ K, $\log g = 5.5$, [M/H] = +0.5 (right). Both models are rotationally broadened by 8 km s^{-1}.

4.2 The potassium doublet

The K I λλ7665, 7699 lines show a clear core reversal (see Fig. 7). This is due to the chromospheric activity of VB 10. The doublet is a resonance transition and thus will be strongly influenced by chromospheric activity. Since we are not treating the chromospheric effects here, our models can only reproduce the line wings which are formed deeper in the photosphere.

As in the case of the sodium lines, both models fit equally well and a distinction between the two parameter sets of $\log g = 5.0$ and [M/H] = 0.0 and of $\log g = 5.5$ and [M/H] = +0.5 is not readily possible (see Fig. 7). The fit itself is not as good as in the case of the sodium doublet, as the models show many more molecular lines. This spectral region is partially contaminated by the telluric O_2 A bands present between 7595 and 7680 Å which we did not remove from the observed data. They are affecting the observations by decreasing the continuum flux to an extent that is not readily known. In addition, this part of the spectrum is dominated by the ε-band of TiO for which the line data are of lower quality (AHS96). Nevertheless, the lines are so broad that we still can fit them as shown in Fig. 7.

4.3 The calcium line

The Ca I λ6573 resonance line also shows chromospheric features as can be seen in Fig. 8. The line is weak and very much filled up, and is hardly detectable without a specific identification. Calcium, in contrast to the two elements discussed above, is not an alkali metal. This means that the vdW damping constant is calculated including the correction factor introduced in equation (5). Although it is hard to compare this weak line with models, we find that the correction factor is necessary in order to reproduce the observed linewidth with the same model parameters as used for the sodium and potassium lines. Without $C_6^{\rm corr}$ the theoretical line profile of the Ca I lines is not broad enough; however, we cannot say how accurate our value for $C_6^{\rm corr}$ is. In order to make a more accurate determination of this factor, we will have to investigate much stronger non-alkali lines with clearer and broader wings. This will be done in a subsequent analysis.

This line cannot be used to determine directly the parameters of VB 10. However, it can be used to confirm them. As in the case of sodium and potassium above, the two models with $\log g = 5.0$, [M/H] = 0.0 and $\log g = 5.5$, [M/H] = +0.5 produce equally good results.

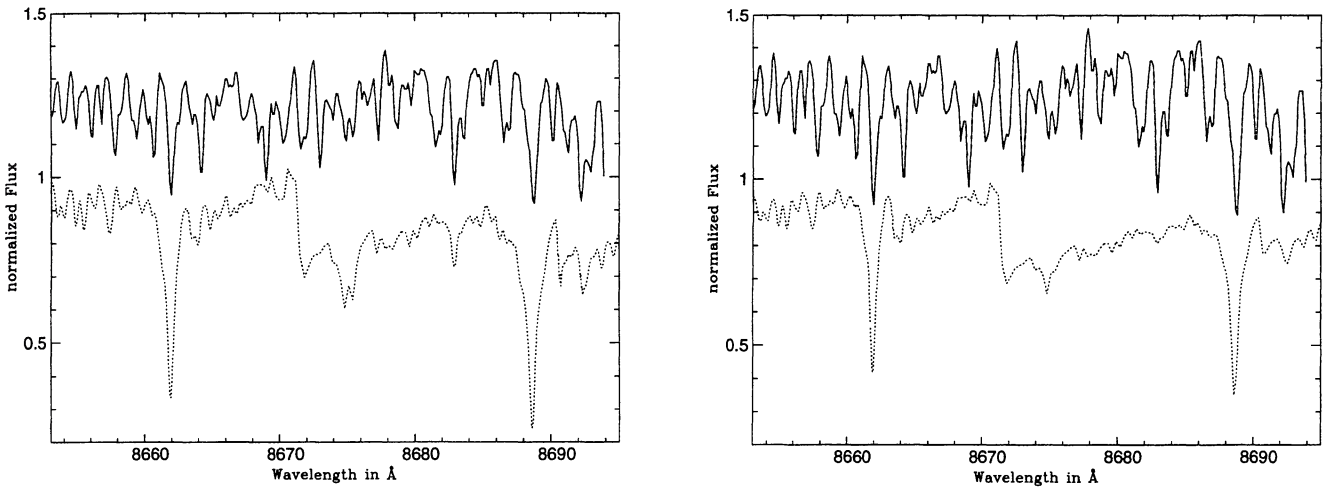

Figure 10. The Fe I λ8662 and Fe I λ8689 lines. Solid: observed. Dotted: $T_{\rm eff} = 2700$ K, $\log g = 5.0$, [M/H] = 0.0 (left); and $T_{\rm eff} = 2700$ K, $\log g = 5.5$, [M/H] = +0.5 (right). Both models are rotationally broadened by 8 km s^{-1}. There has been an offset applied to the observed spectrum. See text for details.

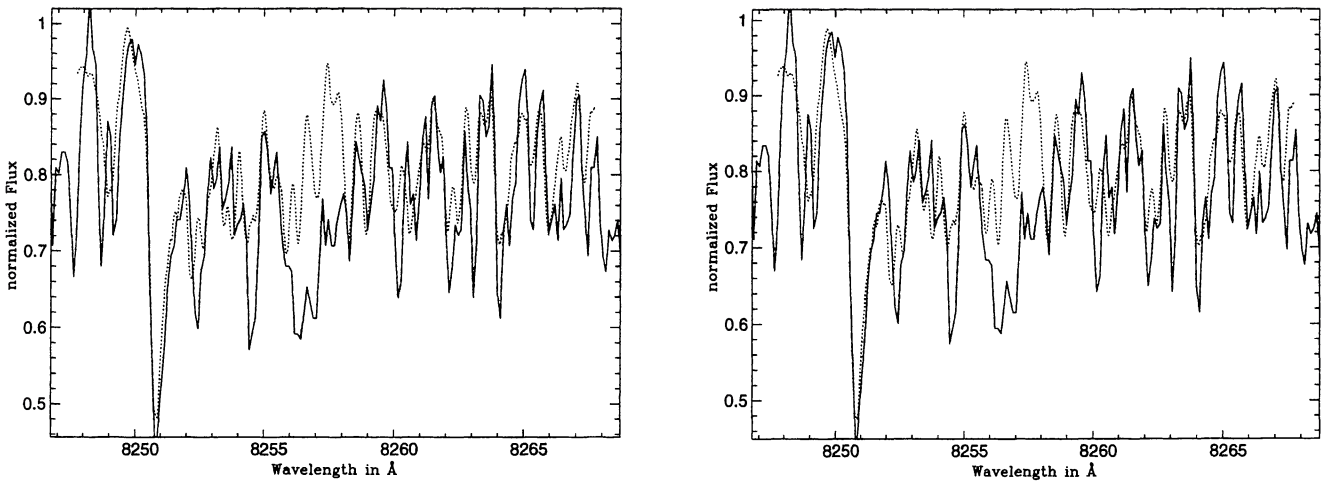

Figure 11. Molecular lines. Solid: observed. Dotted: $T_{\rm eff} = 2700$ K, $\log g = 5.0$, [M/H] = 0.0 (left); and $T_{\rm eff} = 2700$ K, $\log g = 5.5$, [M/H] = +0.5 (right). Both models are rotationally broadened by 8 km s^{-1}.

4.4 The barium line and the iron line at 7913 Å

The fit to the Ba I λ7911 resonance line and the Fe I λ7913 line (which has 0.86-eV excitation energy) is shown in Fig. 9. Both lines are very weak but still visible and we find very good agreement between observations and our two models with $\log g = 5.0$, [M/H] = 0.0 and $\log g = 5.5$, [M/H] = +0.5. As in the case of calcium above, we only used these lines to confirm our range of fitting parameters, since the linewidths are not dominated by the wings of the profiles. They are dominated by their Gaussian cores but the Voigt profiles need to be included in order to lift the cores.

Both metals, barium and iron, are non-alkali metals as is calcium above, and therefore are treated with $C_6^{\rm corr}$ from equation (5). Although the lines are narrow, we find it also necessary here to include such a correction factor in order to fit all lines consistently. However, we cannot make any accurate determinations of $C_6^{\rm corr}$, which still has to be done with stronger lines.

We also point out the very good fit of the surrounding molecular lines (see also Section 4.6).

4.5 The iron lines at 8662 and 8689 Å

The two subordinate Fe I λ8662 and Fe I λ8689 lines visible in the observations are shown in Fig. 10. The lines are not very strong, yet they can be clearly identified. This spectral region is strongly contaminated by terrestial absorption features which reduce the total flux and suppress the molecular pseudo-continuum. Therefore we did not try to fit the lines in detail. Instead we show them with an offset to demonstrate the resemblance of the line shapes of the two Fe I lines.

We cannot use these lines to determine the parameters of VB 10. As in the cases above we used models with $\log g = 5.0$, [M/H] = 0.0 and $\log g = 5.5$, [M/H] = +0.5, and found consistency within the given constraints. Again, calculating the vdW damping constant including $C_6^{\rm corr}$ (see also Section 4.4) results in consistent synthetic spectra. However, due to the uncertainties in the observed spectrum we did not try to determine the accuracy of $C_6^{\rm corr}$ here either.

We point out the 'edge' at approximately 8671 Å in our models, which is due to an abrupt end of a VO band. In our models we can treat VO only with the Just Overlapping Line Approximation (JOLA) method (AH95; AHS96) since no line list is yet available. Since the JOLA method will produce these edges, it is not suitable for computing high-resolution spectra. We point out that the Fe I λ8662 line is slightly contaminated by a Ca II λ8662 line.

4.6 Molecular lines

As mentioned before, the high-resolution spectra are full of a large number of weak molecular lines. For TiO, we use the semi-empirical line list of Jørgensen (1994), which will not reproduce most of the TiO lines at their exact wavelength or their proper *gf*-value. Nevertheless, many of the lines agree very well with observations. We found an excellent agreement with models of the two parameter sets of $\log g = 5.0$, [M/H] = 0.0 and $\log g = 5.5$, [M/H] = +0.5, as can be seen in Fig. 11. Because of the strong influence of rotational broadening, we only use the molecular lines to confirm the parameters and not to derive them directly. On the other hand, we can derive the rotational velocity a second time by using its strong influence on the profile of the molecular lines. We found that rotational velocities between 7 and 9 km s^{-1} produce very similar fits, whereas applying values beyond this interval results in worse fits. Therefore we can confirm a rotational velocity of 8 ± 1 km s^{-1}.

5 SUMMARY AND CONCLUSIONS

We found that the linewidths caused by pressure broadening due to van der Waals damping are very sensitive to both the gravity and the metallicity. Therefore fitting the lines of high-resolution spectra provides a very important tool to determine these two parameters. Nevertheless, since both parameters influence the linewidths in similar ways, one has to be very careful with the analysis.

From the fits to the lines described above we estimate that VB 10 has a gravity in the range $5.0 < \log g < 5.5$ and a metallicity $0.0 <$ [M/H] < 0.5, based on line broadening considerations alone with an adopted effective temperature of $T_{\rm eff} = 2700$ K (Schweitzer 1995). We will investigate the influence of the effective temperature on the line profiles in subsequent work. However, $\log g = 5.5$ and [M/H] = +0.5 are rather high values and not expected for VB 10 (cf. e.g. Henry & McCarthy 1993), so that the lower parts of the interval are physically more likely.

Our calculations result in damping constants for alkali metals that agree satisfactorily well with the Keck observations. The damping constants for non-alkali metals include the correction factor of $C_6^{\rm corr} = 10^{1.8}$ and lead to line profiles which are consistent with the data. In order to obtain a better value for the correction factor, observations of strong non-alkali lines are required. We calculated synthetic spectra outside the observed spectral range available in this paper in order to find such strong lines, but the only line was a moderately strong Fe I λ8829 line, besides the Rb I λ7800 and Rb I λ7948 lines. The iron lines are stronger in hotter M dwarfs, which would be more suitable for testing the vdW broadening of iron lines. We also find that our damping constants for atomic lines are in broad agreement with the values provided by Kurucz. No error should be expected from uncertainties in the oscillator stengths of the atomic lines, since they are much smaller than any other uncertainties and are well known for the light element lines that we have mostly considered here.

Our analysis of the Keck spectra yields values for the gravity which are consistent with the results of interior calculations for VB 10. The $T_{\rm eff}$, [M/H] and $\log g$ combinations agree reasonably well with evolutionary models for M dwarfs (Burrows et al. 1993; Baraffe et al. 1995). Larger damping constants, e.g. resulting from a different treatment of line broadening, would immediately imply too low a value of $\log g$.

There are still discrepancies between models and observations in some molecular line dominated regions of the spectrum. As mentioned above, we suspect this to be due to the molecular line data. This will be improved in subsequent work. We also will investigate the influence of NLTE effects on M dwarf spectra as well as chromospheric features. In addition, observations of different strong atomic lines in spectral regions where molecular absorption is not dominant and blending is less severe (e.g. beyond 1.18 μm, see also Jones et al. 1996) will clarify the calculations of the damping constants and the use of correction factors.

ACKNOWLEDGMENTS

This paper was based on observations obtained at the W. M. Keck Observatory, which is operated jointly by the University of California and the California Institute of Technology. We express our thanks to J. Krautter, S. Starrfield and I. Appenzeller who made this collaboration possible and supported it. We also thank the referee, H. R. A. Jones, for his very helpful comments. This research has been partially supported by NASA LTSA grants NAGW 4510 and NAGW 2628 and NASA ATP grant NAG 5-3067 to ASU, as well as by NSF grant AST-9217946 to WSU. Parts of the model calculations have been performed on the Cray C90 of the San Diego Supercomputer Center and on the IBM SP2 of the Cornell Theory Center, supported by the NSF. We thank them for a generous allocation of computer time. AS was partially supported by a BAFöG grant. GB thanks the University of California for partial travel support to the Keck Observatory.

REFERENCES

Allard F., 1990, PhD thesis, University of Heidelberg
Allard F., Hauschildt P. H., 1995, ApJ, 445, 433 (AH95)
Anders E., Grevesse N., 1989, Geochim. Cosmochim. Acta, 53, 197
Baraffe I., Chabrier G., Allard F., Hauschildt P. H., 1995, ApJ, 446, L35
Baschek B., Scholz M., 1982, in Hellwege K. S. K.-H., Voigt H. H., eds, Astronomy and Astrophysics, Stars and Star Clusters, Landolt-Börnstein VI2b, Numerical Data and Functional Relationships in Science and Technology. Springer Verlag, Berlin, pp. 91–152
Basri G., Marcy G. W., 1995, AJ, 109, 762
Brett J. M., 1995, A&A, 295, 736
Burrows A., Hubbard W. B., Saumon D., Lunine J. I., 1993, ApJ, 406, 158
Hauschildt P. H., Allard F., Alexander D. R., Schweitzer A., Baron E., 1996, in Strassmeier K. G., Linsky J. L., eds, Proc. IAU Symp. 176, Stellar Surface Structure. Kluwer, Dordrecht, p. 539
Henry T. J., McCarthy D. W., Jr, 1993, AJ, 106, 773
Jones H. R. A., Longmore A. J., Allard F., Hauschildt P. H., 1996, MNRAS, 280, 77
Jones H. R. A., Longmore A. J., Jameson R. F., Mountain C. M., 1994, MNRAS, 267, 413
Jørgensen U. G., 1994, A&A, 284, 179
Kirkpatrick J. D., Kelly D. M., Rieke G. H., Liebert J., Allard F., Wehrse R., 1993, ApJ, 402, 643
Kurucz R. L., 1994, Atomic data for opacity calculations, Kurucz CD-ROM No. 1
Kusch H. J., 1958, Z. Astrophys., 45, 1
Schweitzer A., 1995, Diploma thesis, University of Heidelberg
Unsöld A., 1955, Physik der Sternatmosphären, 2nd edn. Springer-Verlag, Berlin
Weast R. C., ed., 1988, Handbook of Chemistry and Physics, 2nd edn. CRC Press, Boca Raton
Wehrse R., Liebert J., 1980, A&A, 86, 139
Weidemann V., 1955, Z. Astrophys., 36, 101